

C-axis electrical resistivity of $\text{PrO}_{1-a}\text{F}_a\text{BiS}_2$ single crystals

Masanori Nagao^{1,2*}, Akira Miura³, Satoshi Watauchi¹, Yoshihiko Takano², and Isao Tanaka¹

¹University of Yamanashi, Kofu 400-8511, Japan

²National Institute for Materials Science, Tsukuba 305-0047, Japan

³Hokkaido University, Sapporo 060-8628, Japan

*E-mail : mnagao@yamanashi.ac.jp

Abstract

The high anisotropy in $\text{RO}_{1-a}\text{F}_a\text{BiS}_2$ (R denotes a rare-earth element) superconductors demonstrates their potential use as intrinsic Josephson junctions, considering the weak coupling among BiS_2 - $\text{PrO}(\text{F})$ - BiS_2 (superconducting-normal-superconducting) layers along the *c*-axis. We grew $\text{PrO}_{1-a}\text{F}_a\text{BiS}_2$ single crystals using CsCl/KCl flux. The superconducting anisotropies of the grown single crystals were estimated to be approximately 40–50 from the effective mass model. The *c*-axis transport properties

were characterized using single-crystal s-shaped intrinsic Josephson junctions with a focused ion beam. Along the *c*-axis, the crystals showed zero resistivity at 2.7 K and a critical current density of 1.33×10^3 A/cm² at 2.0 K. The current–voltage curve along the *c*-axis displayed hysteresis. The *c*-axis transport measurements under a magnetic field parallel to the *ab*-plane revealed a “lock-in” state due to the Josephson vortex flow, indicating that BiS₂ superconductors are promising candidates for intrinsic Josephson junctions.

Main Text

1. Introduction

The newly developed BiS₂-based layered superconductors Bi₄O₄S₃^{1,2)} and RO_{1-a}F_aBiS₂ (R = La, Ce, Pr, Nd, or Yb)³⁻¹²⁾ have attracted much interest. Superconductivity is induced by carrier doping through the substitution of F at the O site in ROBiS₂. Recently, we have reported on the growth of RO_{1-a}F_aBiS₂ (R = La, Ce, Nd) single crystals by using the CsCl/KCl flux method. Their structures and transport properties along the *ab*-plane were examined.¹³⁻¹⁷⁾ The superconducting anisotropies of RO_{1-a}F_aBiS₂ (R = La, Nd) single crystals have been estimated to be as high as 30 using an effective mass model,¹³⁻¹⁵⁾ which demonstrates their potential use as intrinsic Josephson junctions along the *c*-axis.^{18,19)} Intrinsic Josephson junctions were discovered in high-*T*_c cuprate superconductors. Such junctions emerged in the crystal structures of layered superconductors. Consequently, devices based on self-assembled nano junctions have been achieved. The applications of intrinsic Josephson junctions include terahertz radiation sources²⁰⁾ and quantum bits.^{21,22)} However, there have been no previous experimental reports on intrinsic Josephson junctions along the *c*-axis of BiS₂-based layered superconductors. Thus, their *c*-axis transport properties have attracted much

attention. Additionally, single crystals of $\text{RO}_{1-a}\text{F}_a\text{BiS}_2$ ($\text{R} = \text{Pr}$) have not yet been studied.

In this investigation, we grew $\text{PrO}_{1-a}\text{F}_a\text{BiS}_2$ single crystals with different F concentrations using CsCl/KCl flux and examined their transport properties parallel and perpendicular to the *c*-axis. Furthermore, we evaluated the s-shaped junctions^{23,24)} along the *c*-axis of a $\text{PrO}_{1-a}\text{F}_a\text{BiS}_2$ single crystal.

2. Experimental procedure

Single crystals of $\text{PrO}_{1-a}\text{F}_a\text{BiS}_2$ were grown using CsCl/KCl flux.^{13,15)} The raw materials of Pr_2S_3 , Bi, Bi_2S_3 , Bi_2O_3 , and BiF_3 were weighed with a nominal composition of $\text{PrO}_{1-x}\text{F}_x\text{BiS}_2$ ($x = 0\text{--}0.9$). The molar ratio of the flux was CsCl:KCl = 5:3. 0.8 g of weighed raw materials and 5.0 g of CsCl/KCl flux were mixed in a mortar and sealed in a quartz tube in vacuum. The mixed powder was heated at 800 °C for 10 h, cooled slowly to 600 °C at a rate of 1 °C/h, and then furnace-cooled to room temperature. The quartz tube was opened in air atmosphere, and the flux was dissolved in distilled water in the quartz tube. The products were filtered and washed with distilled water. The structures and compositions of the grown single crystals were evaluated by X-ray diffraction (XRD) analysis using CuK α radiation, scanning electron microscopy (SEM),

and electron probe microanalysis (EPMA). The critical temperatures (T_c) of the grown single crystals were estimated from the magnetization–temperature (M – T) curve under zero-field cooling (ZFC) and field cooling (FC) using a superconducting quantum interface device (SQUID) with an applied magnetic field of 10 Oe parallel to the c -axis. The resistivity–temperature (ρ – T) and current–voltage (I – V) characteristics of the single crystals were measured by the standard four-probe method in the constant current (J) mode using a physical property measurement system (PPMS DynaCool; Quantum Design). The electrical terminals were made of silver paste. We measured the angular (θ) dependence of resistivity (ρ) in the flux liquid state under various magnetic fields (H) and calculated superconducting anisotropy (γ_s) using the effective mass model.^{25–27)} For the c -axis transport measurement, we fabricated s-shaped junctions from a grown single crystal fixed on the SrTiO₃ single-crystal substrate by a three-dimensional (3D) focused ion beam (FIB) etching method using a Ga-ion beam.^{23,24)} The area of the junctions was about $5.4 \times 5.7 \mu\text{m}^2$ in the ab -plane. The thickness of the junctions was about 1.0 μm along the c -axis. Normal-state anisotropy (γ_n) was estimated from the ρ – T characteristics of the as-grown ($J//ab$ -plane) and fabricated ($J//c$ -axis) samples. The sample-position (the angle between the ab -plane and the magnetic field) dependence of the flow voltage (V_{ff}) of the fabricated sample was measured under a magnetic field.

3. Results and discussion

Figure 1 shows a typical SEM image of a $\text{PrO}_{1-a}\text{F}_a\text{BiS}_2$ plate like single crystal, which is around 1–3 mm in size and 20–40 μm thick. The well-developed plane was determined to be the *ab*-plane by XRD measurement. Figure 2 shows the XRD pattern of a well-developed plane in a single crystal grown from a starting powder with a nominal composition of $\text{PrO}_{0.7}\text{F}_{0.3}\text{BiS}_2$. The peak positions are in agreement with those of the $(00l)$ diffraction peaks of $\text{PrO}_{1-a}\text{F}_a\text{BiS}_2$ described in the literature.⁶⁾ The presence of only $(00l)$ diffraction peaks of the $\text{PrO}_{1-a}\text{F}_a\text{BiS}_2$ structure indicates a well-developed *ab*-plane.

Figure 3 shows the $M-T$ curve for single crystals grown from a starting powder with a nominal composition of $\text{PrO}_{0.7}\text{F}_{0.3}\text{BiS}_2$ under ZFC and FC. The Meissner effect was confirmed from the magnetization between 2 and 10 K. T_c was defined in the separation temperature of FC and ZFC curves. The T_c and superconducting volume fraction at 2.0 K were estimated to be 3.8 K and 75%, respectively.

Table I shows the F concentrations of the starting materials, *c*-axis lattice parameters, and T_c and γ_s values of the single crystals. The F concentrations in the starting materials and grown crystals are defined as x and y , respectively. Single crystals

were obtained from the starting materials of $0.1 \leq x \leq 0.8$, but only a small amount of grown single crystals was obtained for $x = 0.1$. The chemical ratio of Pr:Bi:S in the single crystals was determined to be 1.06 ± 0.02 : 1.02 ± 0.03 : 2 by EPMA, and the sulfur concentration was normalized to be 2. The composition of the grown crystals was almost stoichiometric, with a slightly Pr-rich composition. Cs, K, and Cl were not detected in the crystals by EPMA with a minimum sensitivity limit of 0.1 wt%. The value of y in the grown crystals increased to up to 0.26 with increasing x to up to 0.5, and it almost saturated at $x \geq 0.5$. The c -axis lattice parameters of the single crystals ($x > 0.2$) were close to those of polycrystalline samples.²⁸⁾ The c -axis lattice parameters of the grown crystals decreased with increasing x , and they almost saturated at $x \geq 0.4$. These results suggest that the solubility limit of F in PrOBiS₂ crystals is between 0.4 and 0.5, as shown in Fig. 4. The values of y and the c -axis lattice parameters are almost the same between $x = 0.5$ and 0.8. However, the T_c s show deviations of 4.1–4.6 K. We assume that the experimental error caused the deviations of T_c values. Slight changes in the F concentration and/or local structure might affect the transition temperature.¹⁷⁾ The grown single crystals, except those at $x = 0.1$, showed superconducting transitions, and the F concentration in the PrO_{1- a} F _{a} BiS₂ grown crystals increased T_c to up to around 4.5 K.

The θ dependence of ρ was measured at different H values in the flux liquid state to estimate the γ_s values of $\text{PrO}_{1-a}\text{F}_a\text{BiS}_2$ single crystals in accordance with the experimental procedure in Refs. 25 and 26. The reduced field (H_{red}) was calculated using the following equation for an effective mass model:

$$H_{\text{red}} = H(\sin^2\theta + \gamma_s^{-2}\cos^2\theta)^{1/2}, \quad (1)$$

where θ is the angle between the ab -plane and the magnetic field,²⁷⁾ and H_{red} is calculated from H and θ . γ_s was estimated from the best scaling of the $\rho-H_{\text{red}}$ relationship. Figure 5 shows the θ dependence of ρ in the grown crystal of $y = 0.18$ under different magnetic fields ($H = 0.1\text{--}9.0$ T) in the flux liquid state at 3.0 K. The $\rho-\theta$ curve exhibits a two-fold symmetry. Figure 6 shows the $\rho-H_{\text{red}}$ scaling obtained from the $\rho-\theta$ curves in Fig. 5 using Eq. (1). The scaling was performed by taking $\gamma_s = 58$, as shown in Fig. 6. Table I shows the superconducting anisotropies of $\text{PrO}_{1-a}\text{F}_a\text{BiS}_2$ single crystals with various F concentrations. The γ_s values of the single crystals were calculated to be 20–58, and the high values of 53–58 were found in the single crystals of $x = 0.3$. This value is higher than that of a $\text{YBa}_2\text{Cu}_3\text{O}_a$ (Y-123) high- T_c cuprate superconductor ($\gamma_s = 45.8$), which shows intrinsic Josephson junctions.²⁹⁾ Thus, the $\text{PrO}_{1-a}\text{F}_a\text{BiS}_2$ single crystals of $x = 0.3$ were employed for the fabrication of s-shaped intrinsic Josephson junctions, as described below.

Figure 7 shows a scanning ion microscopy (SIM) image of the s-shaped junctions fabricated on the $\text{PrO}_{1-a}\text{F}_a\text{BiS}_2$ single crystals of $x = 0.3$ along the c -axis. The cross-sectional area and thickness of the junctions are $5.4 \times 5.7 \mu\text{m}^2$ along the ab -plane and $1.0 \mu\text{m}$, respectively. The direction of current flow is shown in Fig. 7, which is along the c -axis in the junction. This junction was used for characterizing the transport properties along the c -axis. Figure 8 shows the $\rho-T$ characteristics along the (a) ab -plane (ρ_{ab}) and (b) c -axis (ρ_c) of a $\text{Pr}_{1.05}\text{O}_{0.82}\text{F}_{0.18}\text{Bi}_{1.03}\text{S}_{2.00}$ ($y = 0.18$) single crystal, as measured by a standard four-probe method. The zero-resistivity temperature (T_c^{zero}) along the ab -plane was determined to be 2.95 K, whereas that along the c -axis decreased slightly to 2.70 K. Ga ions were likely implanted in the fabricated sample during the FIB etching, which possibly degraded the sample. This decrease in T_c^{zero} may be attributed to the damage caused by FIB etching. The normal-state anisotropies $\gamma_n = (\rho_c/\rho_{ab})^{1/2}$ for $\text{Pr}_{1.05}\text{O}_{0.82}\text{F}_{0.18}\text{Bi}_{1.03}\text{S}_{2.00}$ single crystals at 5 and 250 K were found to be 39.3 and 21.1, respectively. These results suggest that this layered compound shows a highly anisotropic transport even in the normal state. These γ_n values were lower than the γ_s values. The $\rho-T$ relationship along the ab -plane ($J//ab$ -plane) exhibits an anomaly at approximately 140 K and small kinks at ~ 70 K. The former anomaly is similar to those observed in $\text{NdO}_{1-a}\text{F}_a\text{BiS}_2$ and $\text{LaO}_{1-a}\text{F}_a\text{BiSe}_2$ single crystals,^{13,30} in which

temperature may be related to F concentration.³⁰⁾ Thus, those anomalies would be intrinsic properties of BiS₂- and BiSe₂-based superconductors.³⁰⁾ The small kinks at ~70 K along the *ab*-plane ($J//ab$ -plane) and *c*-axis ($J//c$ -axis) are reproducible; however, in origin is unclear.

Figure 9 shows the *I*–*V* characteristics along the *c*-axis of the Pr_{1.05}O_{0.82}F_{0.18}Bi_{1.03}S_{2.00} single crystal (shown in Fig. 7) at 2.0 K when T/T_c was around 0.74. The critical current density (J_c) was approximately 1.33×10^3 A/cm² in the self-field. The *I*–*V* curve shows a hysteresis. However, the multi branch structure of the *I*–*V* characteristics that corresponds to intrinsic Josephson junctions^{23,24)} was not observed in the s-shaped Pr_{1.05}O_{0.82}F_{0.18}Bi_{1.03}S_{2.00} single-crystal junctions.

We measured the sample-position (the angle between the *ab*-plane and the magnetic field) dependence of the V_{ff} characteristics under a magnetic field (H) for s-shaped Pr_{1.05}O_{0.82}F_{0.18}Bi_{1.03}S_{2.00} single-crystal junctions (Fig. 10). We defined flow resistance as V_{ff} divided by dc bias current (I) to conduct the measurements. Figure 10 shows the sample-position dependence of the V_{ff} characteristics at various I_s along the *c*-axis of the s-shaped junctions in a 1.0 T magnetic field at 2.0 K. Figure 10(b) shows that V_{ff} reaches a local maximum under a magnetic field parallel to the *ab*-plane. The local maximum V_{ff} increases with increasing applied current. An increase in the local

maximum V_{ff} is also observed in the I - V characteristics under a magnetic field parallel to the ab -plane, as shown in Fig. 10(c). This phenomenon can be explained by the “lock-in” state,^{31,32)} which may originate from the Josephson vortex flow. We expect that pancake vortices appear in $\text{Pr}_{1.05}\text{O}_{0.82}\text{F}_{0.18}\text{Bi}_{1.03}\text{S}_{2.00}$ single crystals owing to the high superconducting anisotropy. V_{ff} markedly decreases under magnetic fields approximately parallel to the ab -plane, suggesting the dissipation of pancake vortices. Subsequently, Josephson vortices appear under magnetic fields parallel to the ab -plane, indicating the “lock-in” state. The lock-in state is expected to be free from pancake vortices, which cross the superconducting BiS_2 layers. We observed periodic oscillations of Josephson-vortex flow resistance.^{29,33,34)} The starting field of the periodic oscillations (H_s) was calculated from the following equation:^{29,35)}

$$H_s = \Phi_0 / 2\pi\lambda_j s, \quad (2)$$

where $\lambda_j = \gamma_s s$ expresses the size of the nonlinear Josephson-vortex core along the c -axis (frequently called the “Josephson penetration depth λ_j ”), s is the length of a unit cell (= c -axis lattice constant of $\text{Pr}_{1.05}\text{O}_{0.82}\text{F}_{0.18}\text{Bi}_{1.03}\text{S}_{2.00}$), and Φ_0 is the flux quantum (= 2.07×10^{-15} Wb). H_s was calculated from Eq. (2) and was estimated to be 3.12 T for the s-shaped $\text{Pr}_{1.05}\text{O}_{0.82}\text{F}_{0.18}\text{Bi}_{1.03}\text{S}_{2.00}$ single-crystal junctions. However, no oscillation was observed until 7.0 T at 2.0 K. The absence of oscillation may be attributed to the

measurement temperature; T/T_c is around 0.74 at 2.0 K. Although our results demonstrate that $\text{Pr}_{1.05}\text{O}_{0.82}\text{F}_{0.18}\text{Bi}_{1.03}\text{S}_{2.00}$ single crystals are promising candidates for use as intrinsic Josephson junctions, further investigations at lower temperatures are required.

4. Conclusions

We grew $\text{PrO}_{1-a}\text{F}_a\text{BiS}_2$ single crystals with well-developed *ab*-planes 1–3 mm in size using CsCl/KCl flux. Increasing the F concentrations of the starting materials enhanced the substitution of F in the grown crystals. The superconducting T_c and γ_s values of $\text{PrO}_{1-y}\text{F}_y\text{BiS}_2$ ($y = 0.05\text{--}0.28$) single crystals were estimated to be 2.4–4.6 K and 20–58, respectively. The normal-state anisotropies (γ_n) of $\text{Pr}_{1.05}\text{O}_{0.82}\text{F}_{0.18}\text{Bi}_{1.03}\text{S}_{2.00}$ ($x = 0.3$, $y = 0.18$) single crystals at 5 and 250 K were found to be 39.3 and 21.1, respectively. The s-shaped $\text{Pr}_{1.05}\text{O}_{0.82}\text{F}_{0.18}\text{Bi}_{1.03}\text{S}_{2.00}$ single-crystal junctions under a magnetic field parallel to the *ab*-plane exhibited a lock-in state at 2.0 K.

References

- 1) Y. Mizuguchi, H. Fujihisa, Y. Gotoh, K. Suzuki, H. Usui, K. Kuroki, S. Demura, Y. Takano, H. Izawa, and O. Miura, Phys. Rev. B **86**, 220510(R) (2012).
- 2) S. Kumar Singh, A. Kumar, B. Gahtori, G. Sharma, S. Patnaik, and V. P. S. Awana, J. Am. Chem. Soc. **134**, 16504 (2012).
- 3) Y. Mizuguchi, S. Demura, K. Deguchi, Y. Takano, H. Fujihisa, Y. Gotoh, H. Izawa, and O. Miura, J. Phys. Soc. Jpn. **81**, 114725 (2012).
- 4) V. P. S. Awana, A. Kumar, R. Jha, S. Kumar Singh, A. Pal, Shruti, J. Saha, and S. Patnaik, Solid State Commun. **157**, 21 (2013).
- 5) J. Xing, S. Li, X. Ding, H. Yang, and H.-H. Wen, Phys. Rev. B **86**, 214518 (2012).
- 6) R. Jha, A. Kumar, S. Kumar Singh, and V. P. S. Awana, J. Supercond. Novel Magn. **26**, 499 (2013).
- 7) S. Demura, Y. Mizuguchi, K. Deguchi, H. Okazaki, H. Hara, T. Watanabe, S. J. Denholme, M. Fujioka, T. Ozaki, H. Fujihisa, Y. Gotoh, O. Miura, T. Yamaguchi, H. Takeya, and Y. Takano, J. Phys. Soc. Jpn. **82**, 033708 (2013).
- 8) R. Jha, A. Kumar, S. Kumar Singh, and V. P. S. Awana, J. Appl. Phys. **113**, 056102 (2013).

- 9) D. Yazici, K. Huang, B. D. White, A. H. Chang, A. J. Friedman, and M. B. Maple, *Philos. Mag.* **93**, 673 (2013).
- 10) G. Kalai Selvan, M. Kanagaraj, S. Esakki Muthu, R. Jha, V. P. S. Awana, and S. Arumugam, *Phys. Status Solidi: Rapid Res. Lett.* **7**, 510 (2013).
- 11) C. T. Wolowiec, D. Yazici, B. D. White, K. Huang, and M. B. Maple, *Phys. Rev. B* **88**, 064503 (2013).
- 12) B. Li, Z. W. Xing, and G. Q. Huang, *EPL* **101**, 47002 (2013).
- 13) M. Nagao, S. Demura, K. Deguchi, A. Miura, S. Watauchi, T. Takei, Y. Takano, N. Kumada, and I. Tanaka, *J. Phys. Soc. Jpn.* **82**, 113701 (2013).
- 14) J. Liu, D. Fang, Z. Wang, J. Xing, Z. Du, X. Zhu, H. Yang, and H.-H. Wen, *EPL* **106**, 67002 (2014).
- 15) M. Nagao, A. Miura, S. Demura, K. Deguchi, S. Watauchi, T. Takei, Y. Takano, N. Kumada, and I. Tanaka, *Solid State Commun.* **178**, 33 (2014).
- 16) A. Miura, M. Nagao, T. Takei, S. Watauchi, I. Tanaka, and N. Kumada, *J. Solid State Chem.* **212**, 213 (2014).
- 17) A. Miura, M. Nagao, T. Takei, S. Watauchi, Y. Mizuguchi, Y. Takano, I. Tanaka, and N. Kumada, *Cryst. Growth Des.* **15**, 39 (2015).
- 18) R. Kleiner, F. Steinmeyer, G. Kunkel, and P. Muller, *Phys. Rev. Lett.* **68**, 2394

- (1992).
- 19) G. Oya, N. Aoyama, A. Irie, S. Kishida, and H. Tokutaka, *Jpn. J. Appl. Phys., Part 2* **31**, L829 (1992).
- 20) L. Ozyuzer, A. E. Koshelev, C. Kurter, N. Gopalsami, Q. Li, M. Tachiki, K. Kadowaki, T. Yamamoto, H. Minami, H. Yamaguchi, T. Tachiki, K. E. Gray, W.-K. Kwok, and U. Welp, *Science* **318**, 1291 (2007).
- 21) J. Clarke and F. K. Wilhelm, *Nature* **453**, 1031 (2008).
- 22) K. Inomata, S. Sato, K. Nakajima, A. Tanaka, Y. Takano, H. B. Wang, M. Nagao, H. Hatano, and S. Kawabata, *Phys. Rev. Lett.* **95**, 107005 (2005).
- 23) S.-J. Kim, Yu. I. Latyshev, and T. Yamashita, *Appl. Phys. Lett.* **74**, 1156 (1999).
- 24) M. Nagao, M. Sato, H. Maeda, S.-J. Kim, and T. Yamashita, *Appl. Phys. Lett.* **79**, 2612 (2001).
- 25) Y. Iye, I. Oguro, T. Tamegai, W. R. Datars, N. Motohira, and K. Kitazawa, *Physica C* **199**, 154 (1992).
- 26) H. Iwasaki, O. Taniguchi, S. Kenmochi, and N. Kobayashi, *Physica C* **244**, 71 (1995).
- 27) G. Blatter, V. B. Geshkenbein, and A. I. Larkin, *Phys. Rev. Lett.* **68**, 875 (1992).
- 28) R. Jha, H. Kishan, and V. P. S. Awana, *J. Appl. Phys.* **115**, 013902 (2014).

- 29) M. Nagao, S. Urayama, S. M. Kim, H. B. Wang, K. S. Yun, Y. Takano, T. Hatano, I. Iguchi, T. Yamashita, M. Tachiki, H. Maeda, and M. Sato, Phys. Rev. B **74**, 054502 (2006).
- 30) M. Nagao, M. Tanaka, S. Watauchi, I. Tanaka, and Y. Takano, J. Phys. Soc. Jpn. **83**, 114709 (2014).
- 31) K. Kadowaki and T. Mochiku, Physica B **194–196**, 2239 (1994).
- 32) G. Hechtfischer, R. Kleiner, K. Schlenga, W. Walkenhorst, P. Muller, and H. L. Johnson, Phys. Rev. B **55**, 14638 (1997).
- 33) S. Ooi, T. Mochiku, and K. Hirata, Phys. Rev. Lett. **89**, 247002 (2002).
- 34) P. J. W. Moll, X. Zhu, P. Cheng, H.-H. Wen, and B. Batlogg, Nat. Phys. **10**, 644 (2014).
- 35) A. E. Koshelev, Phys. Rev. B **66**, 224514 (2002).

Figure captions

Fig. 1. Typical SEM image of $\text{PrO}_{1-a}\text{F}_a\text{BiS}_2$ single crystal. The well-developed plane is the *ab*-plane.

Fig. 2. XRD pattern of well-developed plane of $\text{PrO}_{1-a}\text{F}_a\text{BiS}_2$ single crystal grown from starting powder with nominal composition of $\text{PrO}_{0.7}\text{F}_{0.3}\text{BiS}_2$.

Fig. 3. *M-T* curve for single crystals grown from starting powder with nominal composition of $\text{PrO}_{0.7}\text{F}_{0.3}\text{BiS}_2$ under ZFC and FC.

Fig. 4. Dependence of starting materials' nominal F composition *x* on (a) analytical F composition *y* and (b) *c*-axis lattice parameter.

Fig. 5. Angular θ dependence of resistivity ρ in flux liquid state at various magnetic fields for $\text{Pr}_{1.05}\text{O}_{0.82}\text{F}_{0.18}\text{Bi}_{1.03}\text{S}_{2.00}$ single crystal.

Fig. 6. Same data as in Fig. 5; scaling of angular θ dependence of resistivity ρ at reduced magnetic field $H_{\text{red}} = H(\sin^2\theta + \gamma_s^{-2}\cos^2\theta)^{1/2}$.

Fig. 7. SIM image of s-shaped junctions. The cross-sectional area and thickness of the junctions are about $30.78 \mu\text{m}^2$ and $1.0 \mu\text{m}$, respectively.

Fig. 8. $\rho-T$ characteristics of $\text{Pr}_{1.05}\text{O}_{0.82}\text{F}_{0.18}\text{Bi}_{1.03}\text{S}_{2.00}$ single crystal along the (a) *ab*-plane (ρ_{ab}) and (b) *c*-axis (ρ_c). Sample for *c*-axis transport measurement is shown in

Fig. 7.

Fig. 9. I - V characteristics of s-shaped $\text{Pr}_{1.05}\text{O}_{0.82}\text{F}_{0.18}\text{Bi}_{1.03}\text{S}_{2.00}$ single-crystal junctions at 2.0 K and self-field. J_c is about 1.33×10^3 A/cm².

Fig. 10. (a) Sample-position (angle between *ab*-plane and magnetic field) dependence of flow voltage V_{ff} at various currents (I) for s-shaped $\text{Pr}_{1.05}\text{O}_{0.82}\text{F}_{0.18}\text{Bi}_{1.03}\text{S}_{2.00}$ single-crystal junctions under 1.0 T magnetic fields at 2.0 K. (b) Enlargement of sample position approximately parallel to *ab*-plane. (c) I - V characteristics of s-shaped junctions at 2.0 K and 1.0 T magnetic field parallel to *ab*-plane.

Table I. Dependence of nominal F concentration in the starting materials (x) on the analytical F concentration (y), c -axis lattice parameter (c), superconducting transition temperature (T_c), and superconducting anisotropy (γ_s) in the grown single crystals. The ratios of F, x , and y are determined by F/(O+F).

x	y	c (Å)	T_c (K)	γ_s
0	— ^{a)}	— ^{a)}	— ^{a)}	— ^{a)}
0.1	0.05	13.67	— ^{b)}	— ^{b)}
0.2	0.13	13.55	2.4	20
0.3	0.18	13.49	3.8	53-58
0.4	0.23	13.41	4.0	32-46
0.5	0.26	13.39	4.1	42-56
0.6	0.26	13.38	4.3	47
0.7	0.26	13.37	4.4	38-39
0.8	0.28	13.37	4.6	
0.9	— ^{a)}	— ^{a)}	— ^{a)}	— ^{a)}

a): No $\text{PrO}_{1-a}\text{F}_a\text{BiS}_2$ single crystals were obtained. b): Unmeasurable in our system and small crystals.

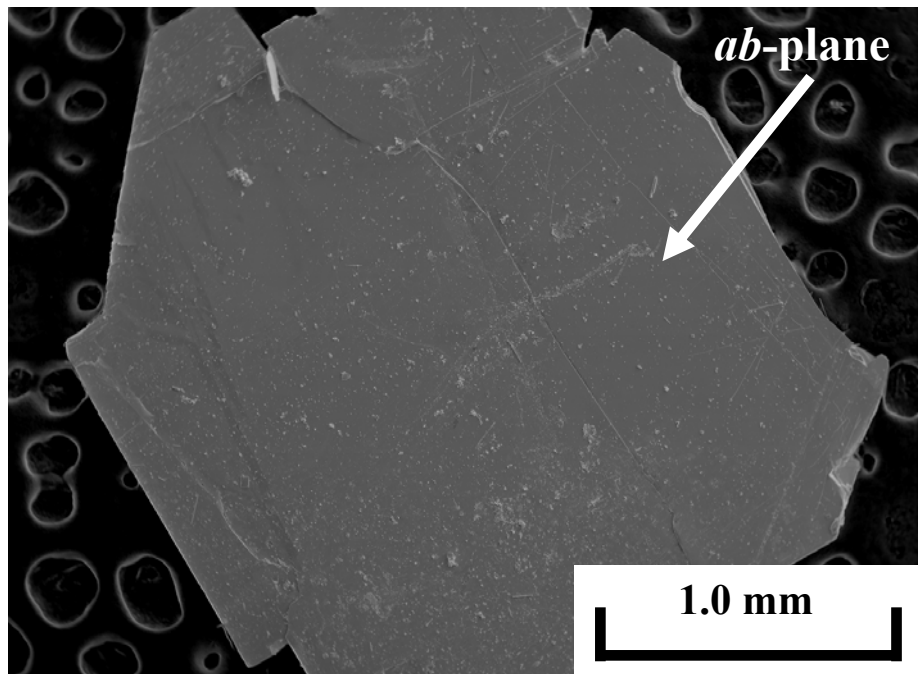


Fig. 1

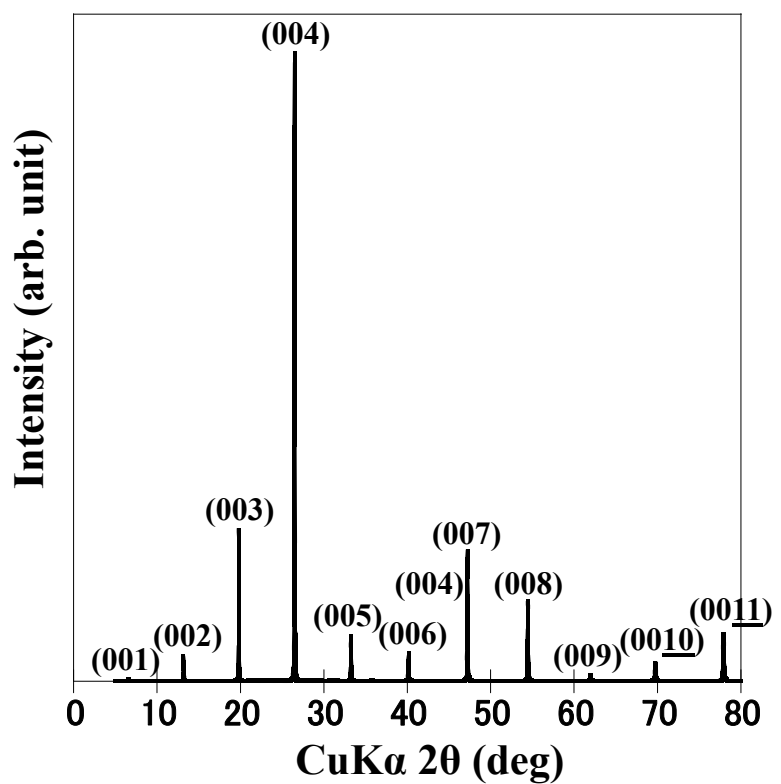


Fig. 2

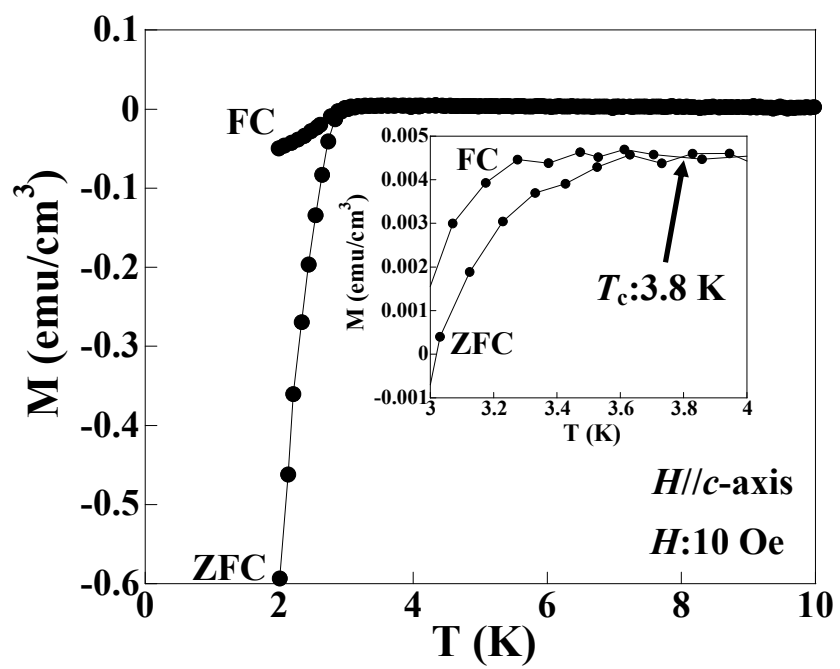


Fig. 3

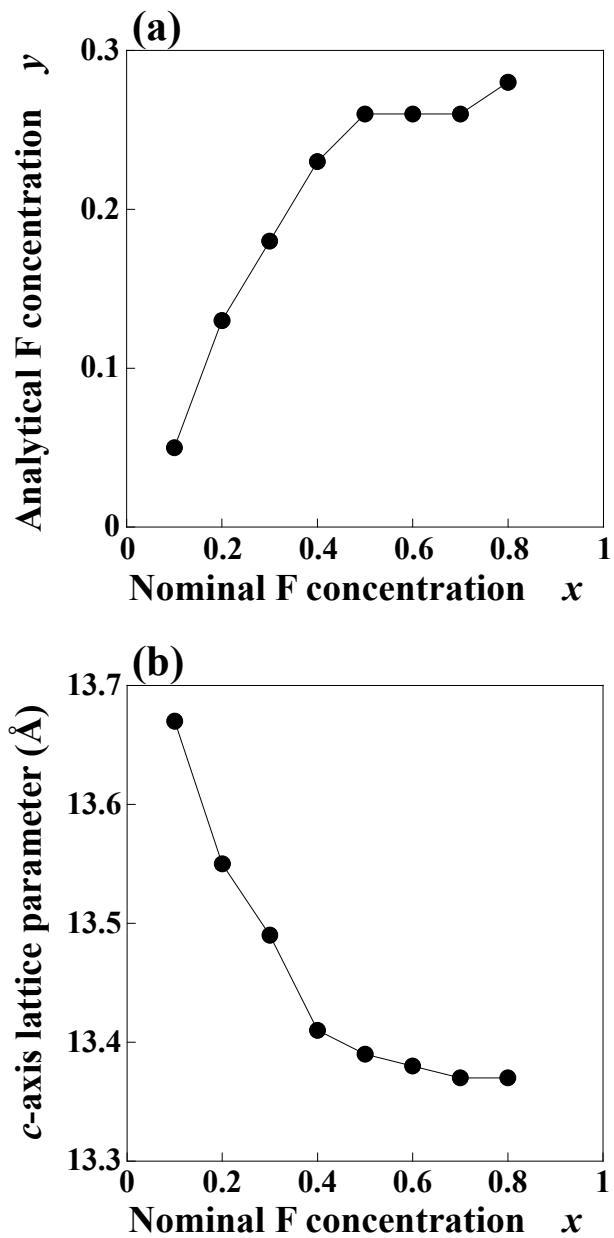


Fig. 4

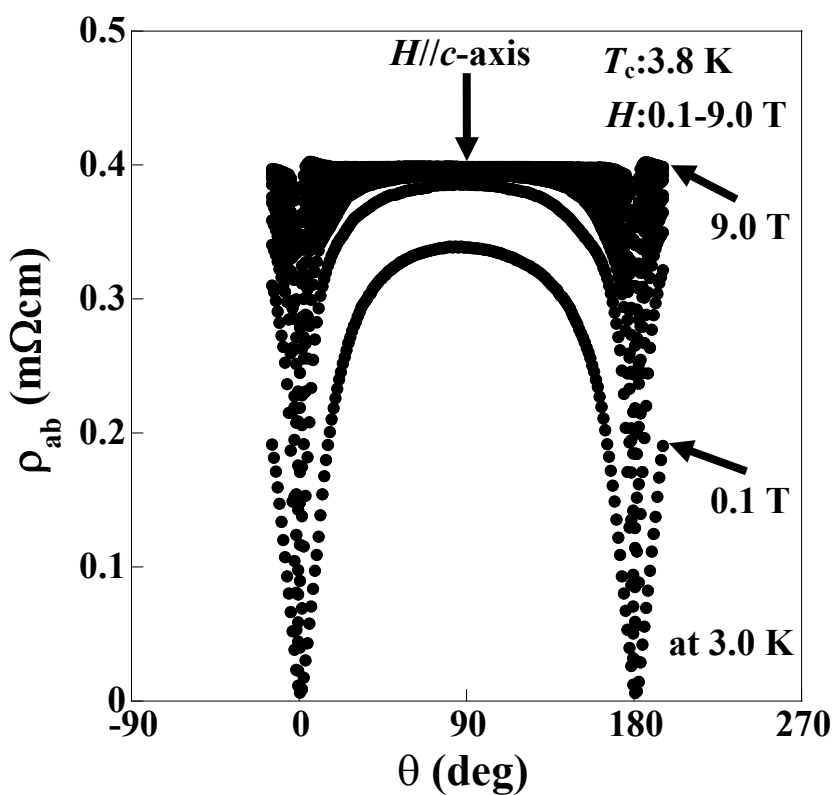


Fig. 5

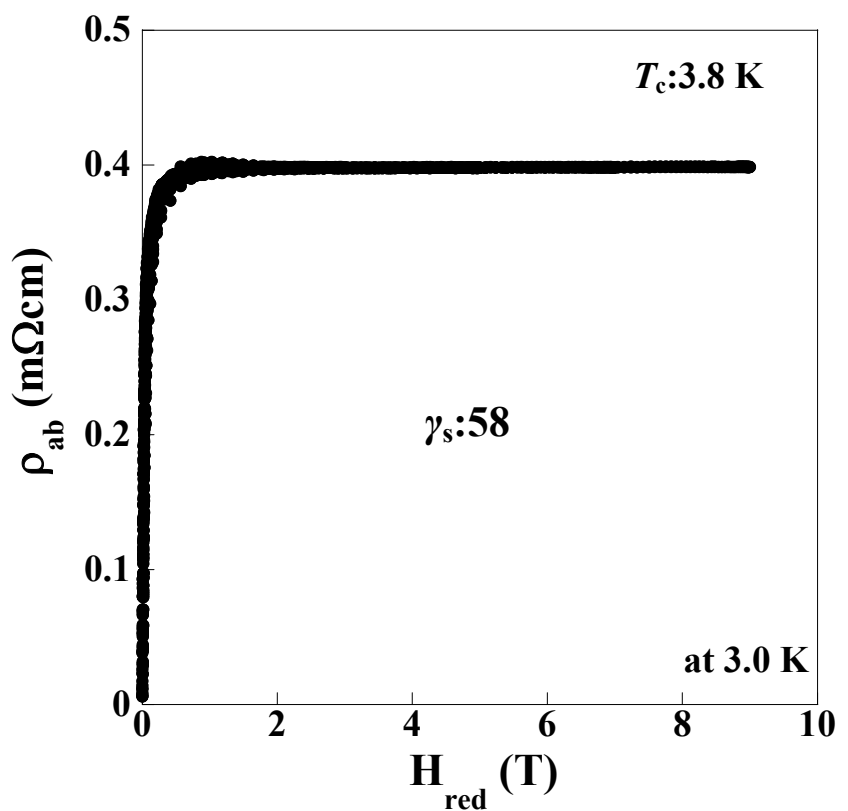


Fig. 6

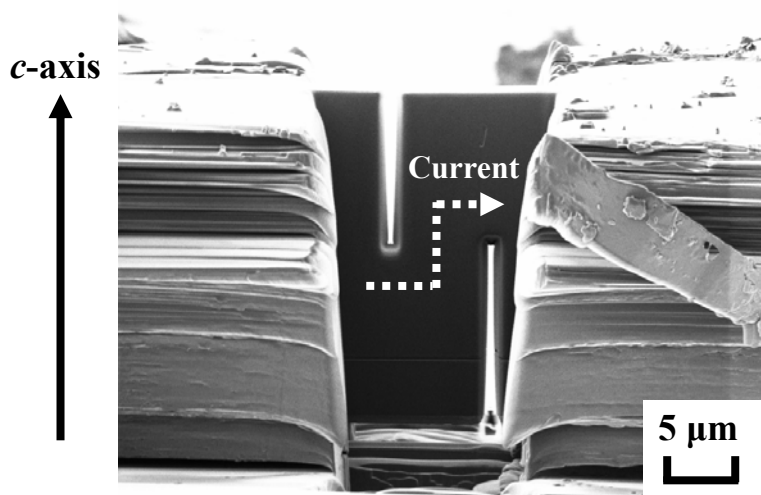


Fig. 7

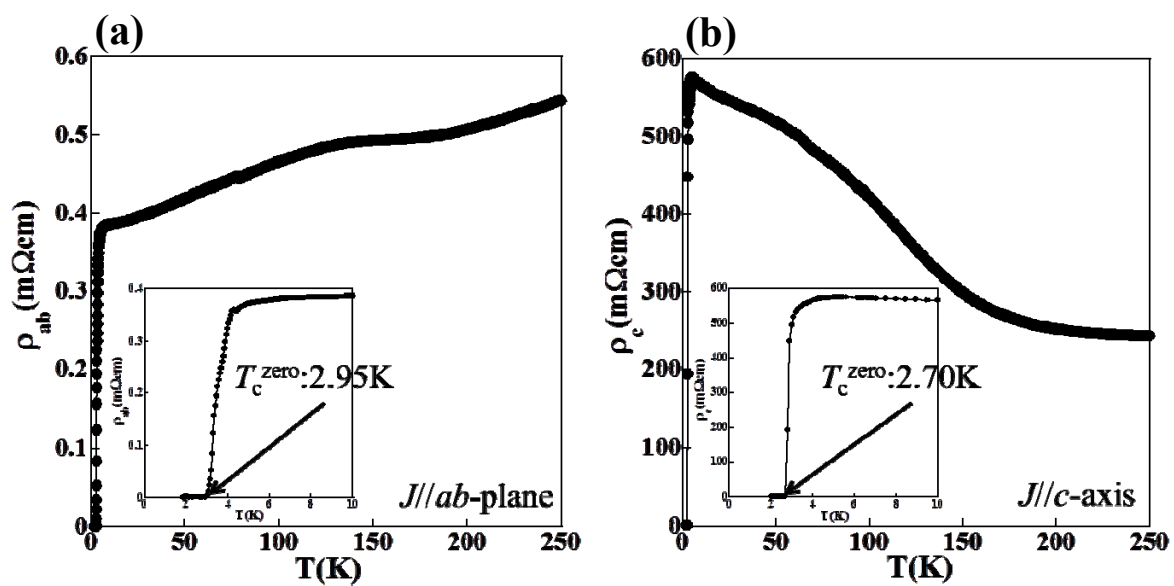


Fig. 8

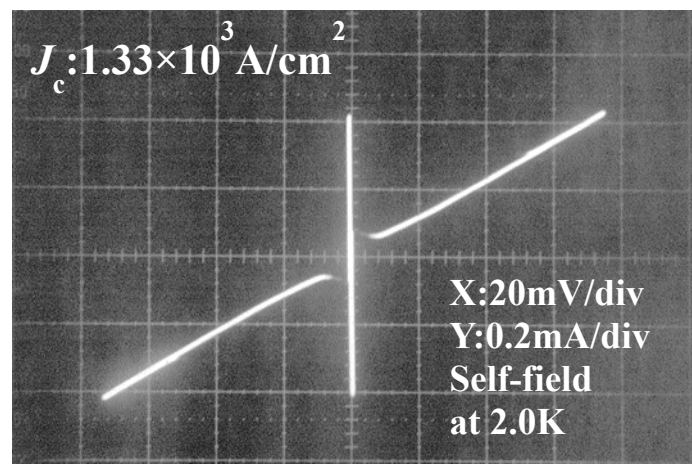


Fig. 9

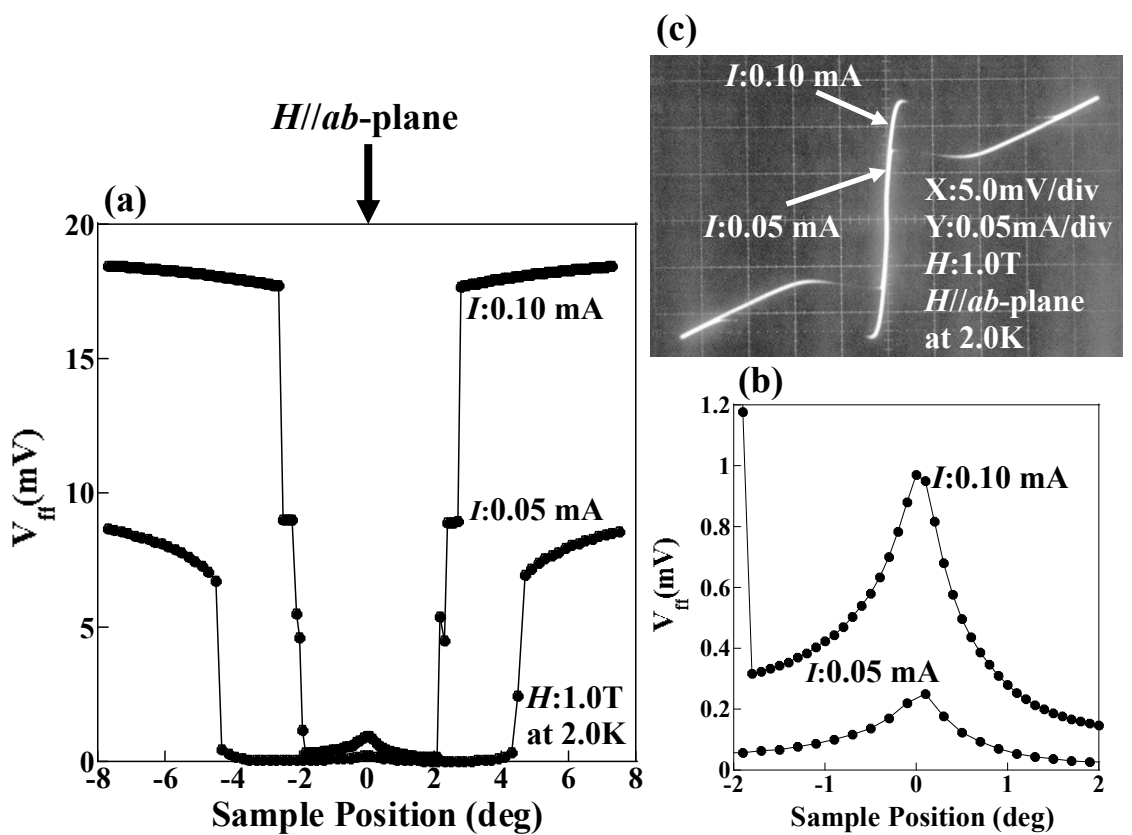


Fig. 10